LANGMUIR

pubs.acs.org/Langmuir
Article

Exfoliation of Cu-Containing Poly(triazine imide): From Three-Dimensional to Two-Dimensional Particle Morphology

Scott McGuigan,[#] Erika Ortega Ortiz,[#] Sungho Jeon, Carrie L. Donley, Eric A. Stach, and Paul A. Maggard*

Cite This: *Langmuir* 2026, 42, 4489−4496

ABSTRACT: Controlling the morphological parameters of extended covalent organic frameworks remains challenging and represents an important yet often elusive metric of consideration. Typically, carbon nitride materials possess local ordering but remain largely amorphous in terms of their long-range order and orientation. This study probes the synthesis of a crystalline carbon nitride, poly(triazine imide) lithium bromide which possesses an atomically-precise extended structure, and demonstrates its exfoliation into a two-dimensional hexagonal sheet-like morphology. Furthermore, a previously unreported carbon nitride material, poly(triazine imide) copper bromide, or PTI-CuBr, was developed through an additional flux-assisted cation-exchange process and is shown to retain its internal Cu cations during solvothermal exfoliation. Characterization by dynamic light scattering and high-angle annular dark-field scanning electron microscopy reveals the morphological changes and captures the high aspect ratio of the thin carbon nitride sheets with <10 nm thickness while maintaining hundreds of nm in width. Additional characterization by energy-dispersive spectroscopy and X-ray photoelectron spectroscopy confirms that the Cu:Br:N molar ratio was maintained within the extended layers throughout the exfoliation process. This top-down synthesis approach differs from typical methods that isolate thin sheets for subsequent metal−cation coordination and illustrates the importance of maintaining oxygen-free conditions to minimize copper clustering. Thus, this new approach is demonstrated to provide a consistent and more homogeneous occupancy of the PTI pore spaces throughout the carbon nitride framework.

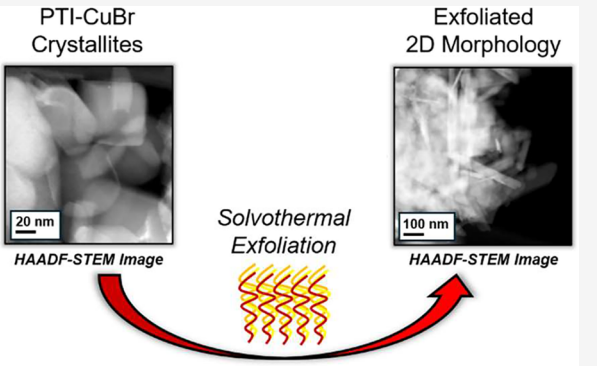

1. INTRODUCTION

Carbon nitride materials act as versatile light absorbing semiconductors for converting photons into photogenerated charge carriers for use in photocatalytic applications.[1] These materials possess advantageous bandgaps and consist of highly durable covalent organic frameworks (COF), enabling them to couple solar absorption with catalytic transformations. This coupling can be accomplished through two primary approaches: surface attachment of molecular catalysts or deposition of metal nanoparticles at specific sites. Both strategies create electron or hole migration centers to facilitate the desired catalytic reactivity. Additionally, polymeric carbon nitrides (PCN) may contain a variety of functional groups that enable tunable interactions within their bulk structures. Recent studies have explored the coordination of different cations and anions within these carbon nitride materials.[2−5] This approach has been most frequently reported for graphitic carbon nitride (g-CN_x) frameworks, which feature a high surface area and molecular-like sp^2 N coordination sites. Within this framework, the PCN structure functions as an extended ligand system containing catalytic metal centers. Importantly, these carbon nitride materials have proven to be effective electrocatalysts for both reductive and/or oxidative processes to desirable products such as H_2, NH_3, reduced carbon products, oxidized carbon products, and O_2.[2,5−9] This versatility makes them valuable for sustainable energy conversion and environmental remediation applications.

More recently, crystalline carbon nitrides that can be synthesized within eutectic salt fluxes have attracted significant interest. These materials exhibit three-dimensional long-range crystalline order around polymeric backbones, which is not typically observed in conventional polymeric carbon nitrides. This work focuses on poly(triazine imide) lithium bromide (PTI-LiBr),[10,11] which exhibits a covalent organic framework structure composed of triazine subunits linked by nitrogen bridges, as illustrated in Figure 1. The framework incorporates well-ordered Li cations and Br anions throughout the

Received: October 1, 2025
Revised: January 1, 2026
Accepted: January 21, 2026
Published: February 3, 2026

https://doi.org/10.1021/acs.langmuir.5c05167
Langmuir 2026, 42, 4489−4496

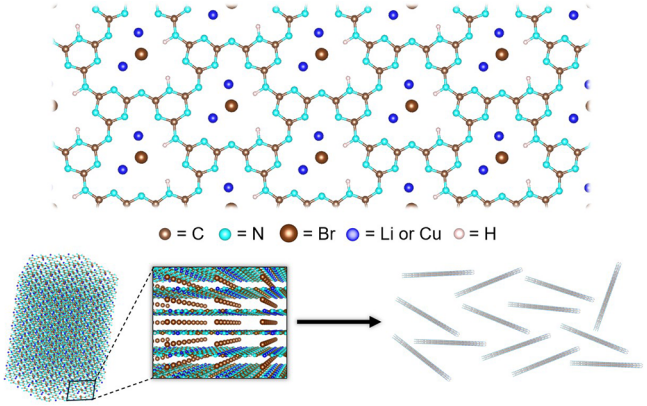

Figure 1. Structural view of a single layer of PTI-LiBr (or PTI-CuBr) and a schematic representation of exfoliating bulk crystalline PTI into a few-layer particle morphology.

crystalline structure. The covalent substructure layer within PTI-LiBr provides a suitable platform for metal-catalyst coordination due to its molecularly precise structural ordering compared to amorphous g-CN_x. These properties have prompted significant efforts aimed at replacing Li cations with metals such as Fe, Mn, and Cu.[6,7,12] Notably, previous work within the Maggard group found that Cu-coordination in the PTI pore spaces enabled reduction of CO_2 to $HCOO^-$ by the carbon nitride at current densities >50 mA·cm^{-2}.[7] The synthetic procedure utilized a flux-assisted cation-exchange reaction that introduced Cu cations within the extended network of PTI-LiCl, thus yielding the new PTI-CuCl.[7] It was found that the complete substitution of the Li sites (2 sites per PTI pore space) by Cu cations could be achieved with a relatively low temperature (290 °C) reaction in a KCl/CuCl flux mixture. However, while thinner particle morphologies were associated with larger current densities, the exfoliation of PTI-CuCl to enhance catalyst-site accessibility has not been reported.

In this study, we aimed to synthetically modify Cu-containing PTI by exfoliating the crystalline material into two-dimensional sheets (Figure 1). This exfoliation process significantly transforms the particle morphology and increases the surface area of the carbon nitride framework, thereby exposing a greater number of intralayer Cu-cation sites. This approach has been previously demonstrated to enhance photocatalytic performance in g-CN_x and PTI-LiCl systems.[13−15] Additionally, we hypothesized that by utilizing the larger bromide anion during the carbon nitride synthesis, the increase in interlayer distance between carbon nitride layers would facilitate its exfoliation. For this purpose, PTI lithium bromide (PTI-LiBr)[10,16,17] was first synthesized and isolated via a flux-mediated reaction, followed by the substitution of Li cations for Cu cations within the structure, yielding PTI copper bromide (PTI-CuBr). Subsequently, a solvothermal exfoliation method was tested on both PTI-LiBr and PTI-CuBr for obtaining few-layer carbon nitride sheets that maintain the crystalline PTI framework.[18] This approach is gentler than acid−based intercalation or framework charging methods,[13,15] allowing the coordinated Cu sites to be maintained within the framework. Thus, this study highlights the critical synthetic parameters to produce few-layer Cu-containing carbon nitride sheets and characterization of the morphological transformation, thereby demonstrating a proof-of-concept for exfoliating crystalline, Cu-containing PTI.

2. EXPERIMENTAL SECTION

2.1. Synthesis of PTI-LiBr

Melamine was ground together with a LiBr (47 mol %) and KBr (53 mol %) eutectic flux at a 1:5 molar ratio of carbon nitride precursor to salt in ambient conditions with a mortar and pestle. Batches were made using 0.4 g of melamine as the starting material. The mixture was then transferred into a 140 °C oven overnight to remove any absorbed moisture. The mixture was ground to eliminate any large chunks and redried before quickly transferring to a fused-silica reaction vessel with ample head space to account for ammonia evolution (~45−50 cm^3). The vessel was sealed under vacuum before reacting inside a box furnace. It was heated to 470 °C (7−8 °C/min) and held at this temperature for 36 h. It was then slowly cooled (2 °C/min) to 320 °C before radiatively cooling to room temperature. The material was removed from the vessel and washed thoroughly with DI water and subsequently with acetone to allow for room temperature drying. Lastly, the product was ground again with a mortar and pestle.

2.2. Synthesis of PTI-CuBr

In an argon glovebox, the synthesized PTI-LiBr was mixed with anhydrous CuBr (68 mol %) and KBr (32 mol %) in a mortar pestle in the presence of excess eutectic flux to facilitate sufficient substitution of the Li sites with Cu (2:3 atom ratio), until the mixture appeared homogeneous. The mix was placed into a fused silica reaction vessel and sealed under vacuum. This was heated at 4−5 °C/min to 290 °C and was held at this temperature for 48 h before the furnace was turned off to radiatively cool. The mixture was then washed thoroughly with DI water before a final wash in acetone for room temperature drying.

2.3. Exfoliation of PTI-LiBr and PTI-CuBr

For all experiments, a three-neck reaction flask with DMAc was heated with stirring until the temperature of the flask reached 60 °C, while ambient air was replaced with N_2 gas during this step. After reaching 60 °C, the carbon nitride material was added (at a 2 mg/mL ratio of carbon nitride to DMAc solvent) and the reaction mixture was further heated to 100 °C. Thereafter, both the N_2 venting and the reaction flask were closed to the outside and allowed to react for 48 h. The heat was then turned off and the mixture was allowed to stir overnight to cool. Once cooled, the solution was removed for centrifugation and decanting separation steps.

2.4. Characterization of PTI-LiBr and PTI-CuBr Materials

The product was characterized using powder X-ray diffraction (PXRD) on a Rigaku R-Axis Spider with CuKα radiation (λ = 1.54056 Å) from a sealed tube X-ray source (40 kV, 36 mA) and a curved image-plate detector. For simulated powder patterns the VESTA software[19] was used and general parameters for the unit cell are listed in the Supporting Information. Fourier-transform infrared spectroscopy (FTIR) was used to collect spectra on a Cary 630 Agilent Spectrometer in the range of 4000−650 cm^{-1}. UV−vis diffuse reflectance (DR) spectra were collected on a Shimadzu UV-3600 UV−vis-NIR spectrophotometer with an integration sphere range of 250−1000 nm. Pressed $BaSO_4$ disks were used as the reflectance background.

2.5. Characterization of Exfoliated Materials

Dynamic Light Scattering (DLS) experiments used a Malvern Zetasizer Nano-ZS and 1 cm glass cuvette. All samples were dispersed in DMAc (~2 mL) with 3 scans averaged per sample. The XPS data was collected on a Kratos Supra+ system with a monochromatic Kα X-ray source operated at 150 W. A charge neutralizer was used to prevent charging when necessary and all spectra were corrected to the C 1s peak at 284.6 eV. Survey and high-resolution scans were acquired at pass energies of 80 and 20 eV, respectively, and the analyzed spot size was 300 × 700 μm. High-angle annular dark-field

https://doi.org/10.1021/acs.langmuir.5c05167
Langmuir 2026, 42, 4489−4496

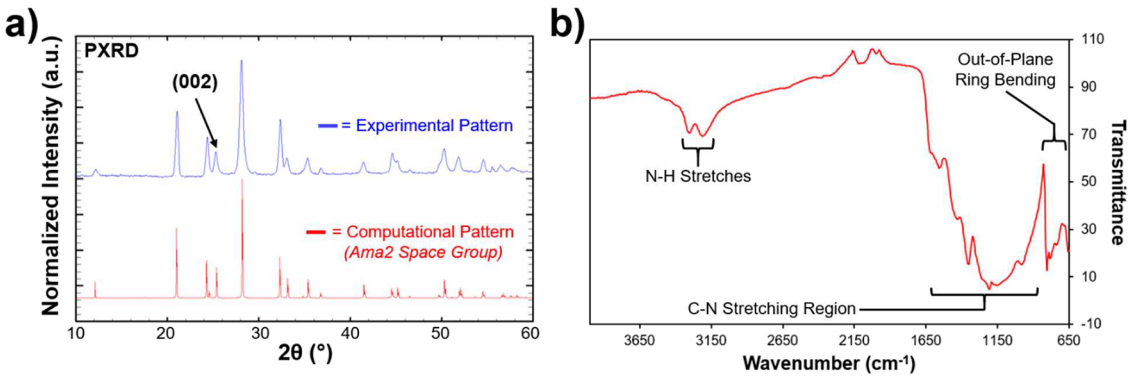

Figure 2. (a) Experimental powder X-ray diffraction pattern of synthesized PTI-LiBr (in blue) and the theoretical pattern (in red) and (b) FTIR signal of synthesized PTI-LiBr.

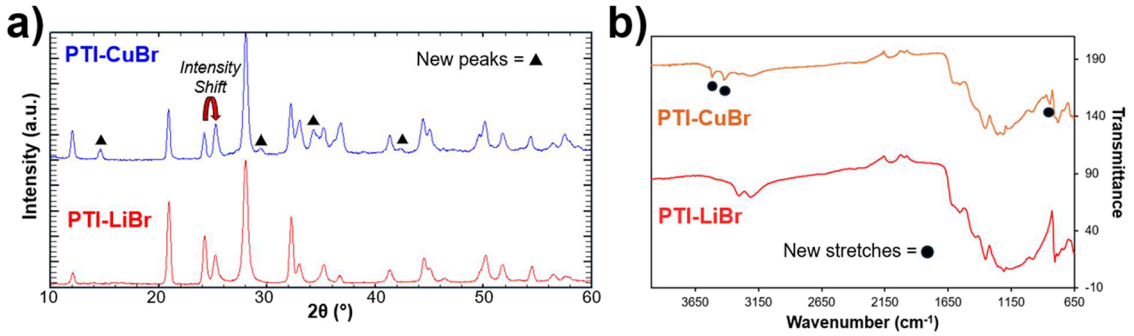

Figure 3. (a) PXRD patterns of synthesized PTI-LiBr (in red) and PTI-CuBr (in blue). (b) FTIR transmittance data from the same two samples in red and orange, respectively.

scanning transmission electron microscopy (HAADF-STEM) and energy-dispersive X-ray spectroscopy (EDS) analyses were performed using a JEOL NEOARM S/TEM operated at an accelerating voltage of 200 kV. The microscope was configured with a 6C probe size, a convergence angle of 27 mrad, and a 40 μm condenser aperture, providing a probe current of approximately 70 pA. For sample preparation, carbon nitride materials were suspended in DMAc. The dispersion was then drop-cast onto a copper TEM grid coated with an ultrathin carbon film, ensuring minimal sample aggregation and optimal electron transparency. This protocol facilitated detailed microstructural and compositional analysis via HAADF STEM and EDS.

3. RESULTS AND DISCUSSION

3.1. Carbon Nitride Synthesis, Exfoliation, and Dynamic Light Scattering

The starting carbon nitride material used in this work, PTI-LiBr, was synthesized via melamine pyrolysis and condensation in a eutectic flux medium (LiBr/KBr). Here, the PTI framework is crystallized with Li cations and Br anions, stabilizing the polymeric framework. X-ray diffraction from this PTI-LiBr framework showed that the material exhibited a crystalline structure consistent with the reported orthorhombic space group,[20] with an (002) reflection at 25.3° yielding a measured *d*-spacing of 3.51 Å (Figure 2a). This reflection was representative of the layer-to-layer stacking distance between the carbon nitride layers. FTIR analysis of the polymeric PTI backbone indicated that the triazine subunits occur in a two-dimensional extended network, most notably characterized by N−H stretches at high wavenumbers (3000−3300 cm^{-1}), the triazine fingerprint stretching region between 900 and 1700 cm^{-1}, and signals at low wavenumbers representing the out-of-plane triazine ring bending modes (shown in Figure 2b).

Incorporation of Cu cations into the PTI matrix was accomplished via a flux-assisted substitution reaction in a second eutectic flux, CuBr/KBr. This reaction was kept at a low reaction temperature of 290 °C (24 h) to ensure that the polymeric backbone remained intact, while the Li cations were replaced by Cu throughout the substitution. The reaction was held at this temperature for 48 h to maximize cation exchange. After cooling, the material was washed and characterized. X-ray diffraction results revealed that the PTI-CuBr retained the characteristic diffraction pattern of PTI-LiBr with minor additional peaks appearing at low intensities (<45°). There was also a shift in intensity associated with the layer-to-layer stacking peak at a 2θ value of 25.3° and its neighbor at 24.4°. This increase in the 25.3° reflection, associated with the layer-to-layer (002) stacking feature, is consistent with the introduction of Cu into the coordination sites within each PTI layer[6,7] thereby increasing the intensity associated with this reflection. The additional minor reflections are not consistent with any specific CuO_x/CuO_xH_y species[21−23] and rather indicate changes from the integration of Cu into the structure. The FTIR spectra from the PTI-CuBr also remained largely unchanged compared with the PTI-LiBr structure, possessing stretching regions consistent with the PTI backbone (Figure 3b). However, like the PXRD analysis there are a few newly introduced signals that suggest there are small changes to the bonding environment. Two of these peaks are located at 3515 and 3420 cm^{-1}. This region is associated with either O−H or N−H bonding interactions. However, the sharpness of these signals is more representative of N−H bonding[24] and suggests small changes in the chemical environment of the

https://doi.org/10.1021/acs.langmuir.5c05167
Langmuir 2026, 42, 4489−4496

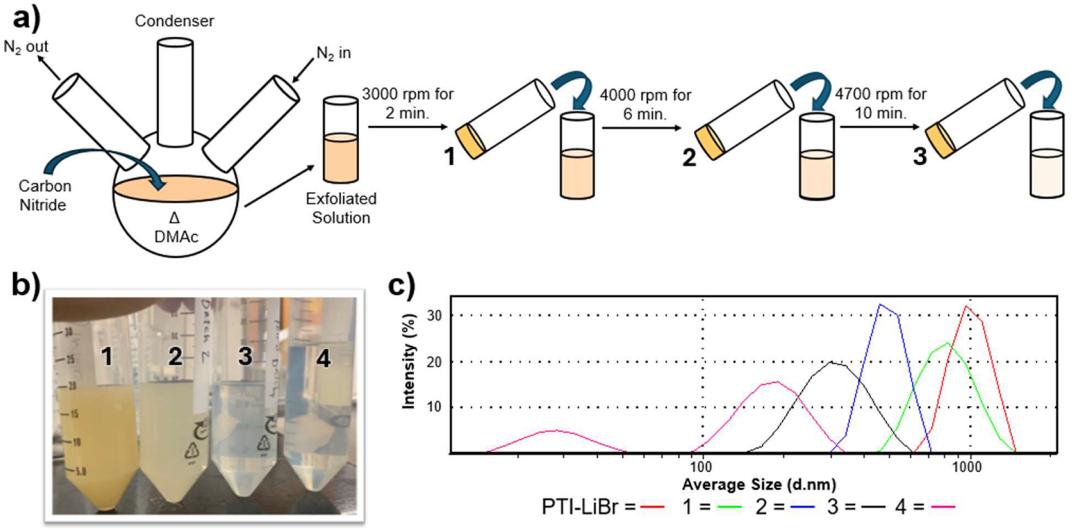

Figure 4. (a) Synthetic exfoliation procedure in heated DMAc followed by centrifugation and decanting, (b) visual image of particle suspensions in DMAc, and (c) DLS particle size data for the materials separated during each of the centrifugation steps.

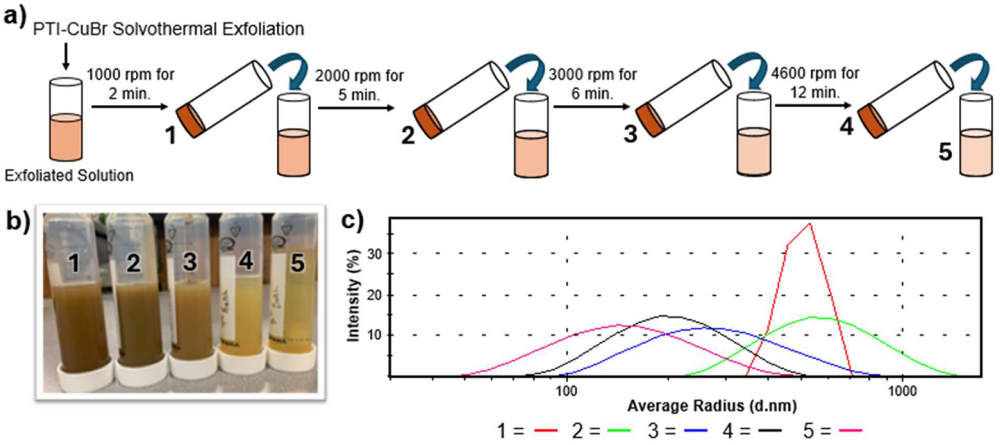

Figure 5. (a) Centrifugation and decanting steps after solvothermal exfoliation for PTI-CuBr, (b) visual image of particles suspended in DMAc, and (c) DLS particle size data for the materials separated from the centrifugation steps.

intralayer pore spaces due to the Cu cations. The other noticeable new signal occurs at 814 cm^{-1}. This signal is sharp and is consistent with out-of-plane ring bending modes, which would also be consistent with Cu introduction into the pore spaces impacting how these modes interact with the framework. Lastly, to confirm the presence of the Cu sites, XPS analysis was conducted to evaluate the Cu 2p signal and the overall elemental composition of the obtained product (Figure S8 and Table S1). The Cu:Br molar ratio was found to be roughly 2.5:1 (16:6.3), slightly higher than expected. Further, the Cu 2p XPS signal is representative of mixed Cu^{+}/Cu^{2+} sites, indicating partial oxidation has occurred. This likely stems from the extensive washing needed to dissolve the residual CuBr from the flux-mediated exchange reaction.

Next, the carbon nitride materials were subjected to exfoliation using a solvothermal procedure in heated dimethylacetamide (DMAc) solution. Once added to the solvent, the suspension was stirred for 48 h at 100 °C to exfoliate the carbon nitride materials. The DMAc solvent acted as a polar aprotic reaction medium. DMAc possesses both organic character to interact with the carbon nitride framework, and a strong polarity from the carbonyl portion of the amide to interact with the coordinated cations. Both aspects are likely key to the exfoliation of the crystalline carbon nitride materials. Without any protic character, there are limited interactions between the solvent and the coordinated ions that may otherwise act to deionize the carbon nitride sheets.[25] The obtained solutions were then subject to a series of centrifugation steps to separate the bulk or least exfoliated portions of the mixture from the more exfoliated and easily suspended particles (Figure 4a). For PTI-LiBr exfoliation, DLS analysis of the separated materials resuspended in DMAc solution (visually shown in Figure 4b) was used to evaluate the average particle sizes and changes. The diameter of the particles remaining suspended was observed to decrease with increased centrifugation speed and time. As shown in Figure 4c, this particle diameter became smaller than 200 nm (average of ∼180 nm diameter) at the smallest particle size detected. This shift equated to a decrease from ∼3.0×10^6 nm^2 of surface area per particle for the starting materials to ∼1.1×10^5 nm^2 (see Table S5) for the thin sheet-like morphology. To examine the influence of interlayer spacing on exfoliation difficulty, the same synthesis procedure was conducted using PTI-LiCl as the starting material. The Cl ion decreases the

https://doi.org/10.1021/acs.langmuir.5c05167
Langmuir 2026, 42, 4489−4496

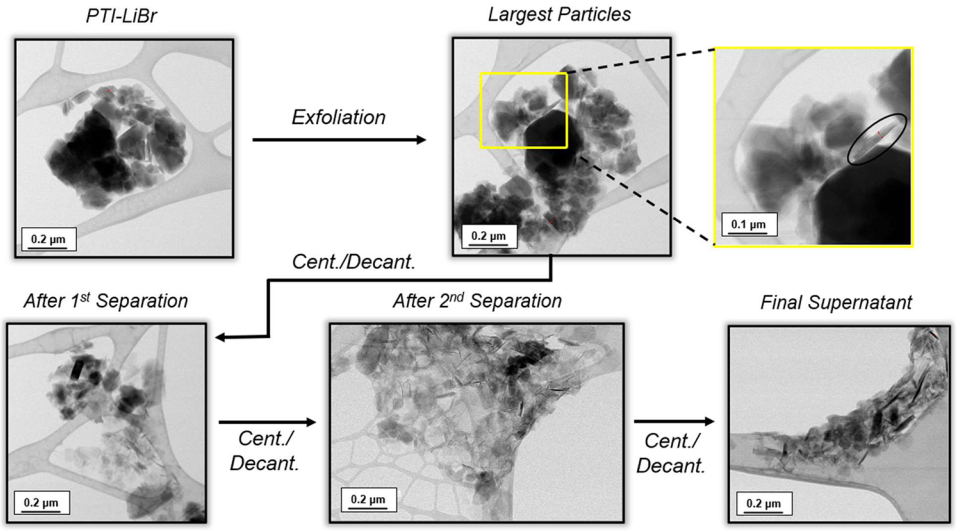

Figure 6. BF-STEM images of the obtained morphology from PTI-LiBr exfoliation. The particles exhibited characteristic decreases in particle size. The final isolated product almost solely resembled 2D sheet-like morphologies after the final separation step (drop-cast from the supernatant for imaging).

interlayer spacing to 3.36 Å, potentially making the material more challenging to exfoliate as compared to PTI-LiBr. As anticipated, the exfoliation of PTI-LiCl was less effective, with DLS showing predominantly larger particles (800−1200 nm diameter) and only minor amounts of smaller exfoliated material in the range of ∼500 nm (Figure S2 in Supporting Information).

The PTI-CuBr material was next subjected to the same exfoliation procedure. The exfoliated material obtained was subjected to a set of particle separation steps, with optimized centrifugation speeds shown in Figure 5a and was subsequently evaluated by DLS (Figure 5c). The range in particle sizes and the amount of exfoliated material increased compared to the prior exfoliation of PTI-LiBr. This is supported by the DLS analysis of the particle size isolated after each centrifugation speed, shown in Figures 4 and 5. For example, an average particle size diameter of ≤260 nm for PTI-LiBr was only detected in the final supernatant after all centrifugation steps were conducted, while this same threshold was achieved when collecting material that settled in solution during the third centrifugation step at 3000 rpm for 6 min in the PTI-CuBr sequence. Furthermore, the multistep separation procedure yielded fractions that could be effectively isolated from solution (Figure 5) with particle sizes <100 nm. Despite the reduced particle sizes, material recovery improved dramatically with 2−20 mg isolated per separation step for the exfoliated PTI-CuBr. In comparison, only small amounts (<10 mg of total sample) could be liberated from the smaller particle-size fractions of the exfoliated PTI-LiBr material remaining after the first centrifugation and decanting step at 3000 rpm for 2 min. This enhanced recovery was attributed to both improved exfoliation efficiency upon Cu coordination and increased bulk density of the Cu-containing framework. Furthermore, the exfoliated PTI-CuBr material detected in the final supernatant, representative of the smallest obtained particles, gave an average particle size of ∼125 nm detected by DLS. This equated to a calculated surface area of 4.9×10^4 nm^2, which was an additional order of magnitude smaller than that found from the exfoliated PTI-LiBr.

3.2. Morphology Characterization of Carbon Nitride Materials

High-angle annular dark-field scanning transmission electron microscopy (HAADF-STEM) was employed to visualize the morphological changes induced by exfoliation and to probe the spatial distribution of Cu within the PTI framework. Prior to exfoliation, both PTI−LiBr and PTI−CuBr samples exhibited dense, polycrystalline morphologies with well-defined lattice planes and hexagonal prism-like crystallites. These features are consistent with the ordered PTI structure and confirm the retention of long-range crystallinity following synthesis.[26−29] Upon solvothermal exfoliation in DMAc, a transformation in morphology was observed. The exfoliated PTI−LiBr samples displayed a progressive breakdown into thinner, needle-like particles with increasing centrifugation steps (Figure 6). After the third separation step, the sample became notably more transparent, reflecting a reduction in bulk mass and the emergence of thinner, needle-like particles each less than 10 nm in thickness and averaging about ∼15.2 nm. A subsequent fourth separation further decreased the particle thickness to ∼14.6 nm. These morphological features are consistent with exfoliation of the bulk crystallites into thinner layers that maintain ∼50−200 nm in width.

Exfoliated PTI−CuBr samples exhibited similar morphological trends, but with even more pronounced thinning. HAADF-STEM images showed the presence of thin, hexagonal flakes with dimensions below 100 nm. Notably, after the exfoliation processes, bright regions were observed (Figure S4) that were absent when imaging the unexfoliated PTI-CuBr. These regions, which appear as localized clusters, were suspected to be Cu-rich domains. To investigate their nature, energy-dispersive X-ray spectroscopy (EDS) mapping was performed in tandem with HAADF-STEM imaging. Elemental maps confirmed that the bright clusters corresponded to regions enriched in both Cu and O, suggesting the formation of CuO_x species (Figure S5). These clusters were observed across the various exfoliation batches/stages but not in the starting material as the Cu clusters seemed to aggregate during exfoliation. This is likely due to residual moisture or oxygen in the DMAc solvent that drives this formation. Electron energy

https://doi.org/10.1021/acs.langmuir.5c05167
Langmuir 2026, 42, 4489−4496

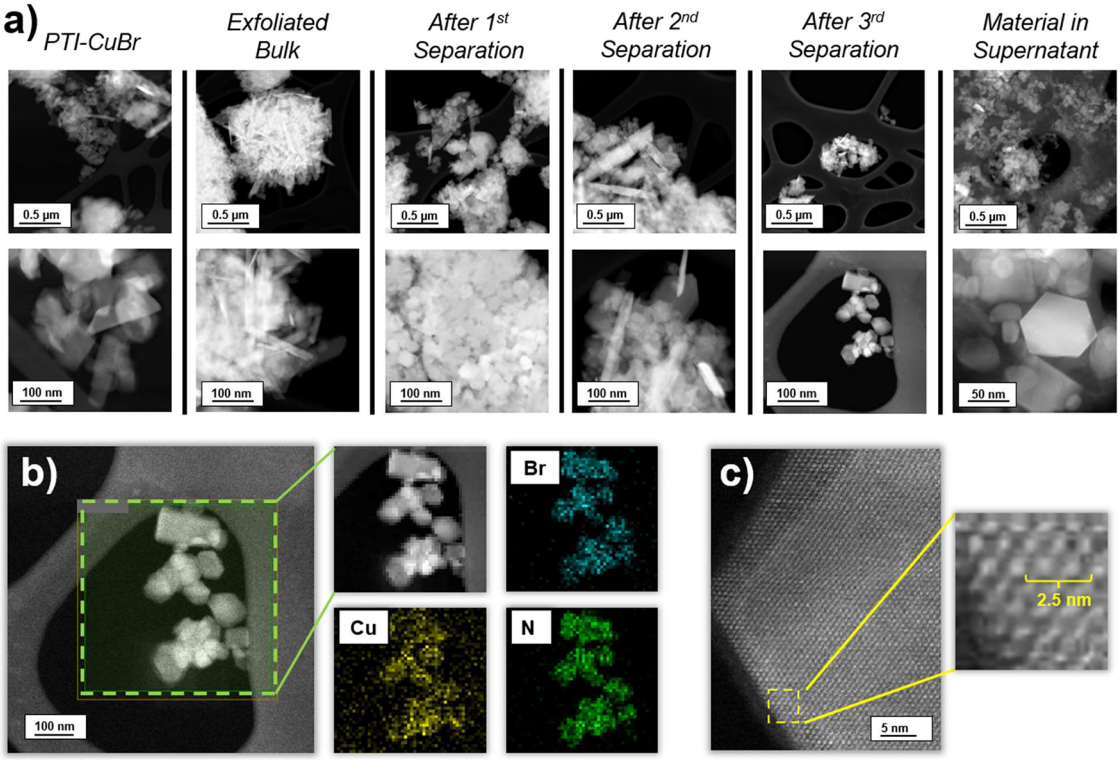

Figure 7. HAADF-STEM imaging. (a) PTI-CuBr and exfoliated PTI-CuBr at each stage of centrifugation separation (high-res and low-res images). (b) EDS analysis of exfoliated PTI-CuBr showing elemental contributions consistent with Cu and Br evenly distributed throughout the polymeric flakes. (c) High-resolution image of the PTI-CuBr flake with a magnified inset displaying the crystalline PTI framework.

loss spectroscopy (EELS) analysis from the clustered formations showed O K-edge peaks at 531 and 535.8 eV, consistent with the Cu spectra of a CuO standard, as shown in the Supporting Information.[30,31]

To address the Cu cluster formation, a modified exfoliation protocol was implemented. The DMAc solvent was dried over 5 Å molecular sieves for 5 days prior to use. Additionally, the solvent was purged vigorously with N_2 along with venting of the Schlenk line setup prior to solvent heating with minimal moisture and oxygen exposure. HAADF-STEM imaging of exfoliated PTI-CuBr prepared under these modified conditions showed no evidence of Cu clusters. The images revealed thin, hexagonal, crystallite flakes throughout (Figure 7a). EDS mapping of these optimized samples further supports the uniform incorporation of Cu and Br within the exfoliated sheets. The elemental maps showed a consistent overlap of Cu and Br signals across the structures, with no localized segregated regions (Figure 7b). This suggests that the Cu cations remained coordinated within the PTI pore spaces during exfoliation, rather than forming separate oxide phases. With close inspection of isolated thin layer sheets, the underlying carbon nitride framework was evaluated. Figure 7c shows the clear geometric patterning of the PTI framework and when compared to the *Ama2* space group using a computational model (Figure S10). The captured alignments are a precise match with the spacing obtained in the STEM analysis. Lastly, selected-area electron diffraction (SAED) demonstrated that the crystallinity of the PTI sheets is maintained (Figure S8). The pattern shows discrete diffraction spots arranged in a symmetrical manner consistent with retention of its crystalline structure.

The elemental content was further confirmed from X-ray photoelectron spectroscopy (XPS) of the exfoliated materials isolated from solution. Acetone was used after each centrifugation step to wash and remove any residual DMAc solvent before drying overnight. As shown in Table S2, all the isolated materials showed the expected Cu:Br (~2:1 molar ratio) content as well as a consistent ratio of Cu:N (~1:3 molar ratio), indicating that the Cu coordination within the extended framework had been maintained. During this synthesis, the most exfoliated particles remaining in the supernatant were unable to be isolated as effectively, and efforts to evaporate or remove the solvent showed elemental content consistent with dried DMAc (Table S3). However, EDS obtained during STEM imaging of the dried supernatant detected Cu, Br, and N consistent with the XPS data for carbon nitride materials. By retaining the Cu cations within the exfoliated carbon nitrides, the amount of Cu surface sites dramatically increased. Using the results from DLS analysis, combined with the density calculated from the crystal structure, the surface area per gram of material was tabulated. As listed in Table S5, the number of particles per gram of the unexfoliated PTI-LiBr was 9.5×10^{11}. After exfoliation, this significantly increased to 1.3×10^{14} particles per gram, or a 133-fold increase, for the smallest particle sizes. This further dramatically increased for the exfoliated PTI-CuBr material to 3.2×10^{15} particles per gram, or an ~337 fold enhancement. The hexagonal faces of the crystalline carbon nitride framework, as found by the electron microscopy results, likely represent the greatest fraction of the increased surface area.

https://doi.org/10.1021/acs.langmuir.5c05167
Langmuir 2026, 42, 4489−4496

4. CONCLUSIONS

A soft exfoliation of Cu-containing PTI materials to produce two-dimensional carbon nitride nanosheets is demonstrated with the maintenance of the coordinated Cu-cations in the intralayer pore spaces of its crystalline structural framework. This approach combines the flux-assisted synthesis of crystalline PTI-LiBr to integrate Cu-cations throughout its structure, followed by a soft solvothermal exfoliation using anhydrous DMAc solvent. Key achievements include the development of an effective size separation protocol that reduced average particle diameters by 80−90% and producing suspended carbon nitride nanosheets in DMAc. XRD analysis confirmed near-complete replacement of Li^+ ions with Cu^+/Cu^{2+} cations using a KBr/CuBr eutectic flux, while maintaining the structural integrity of the PTI framework. The exfoliated materials achieved a thickness of <10 nm while preserving the Cu-coordination within the intralayer pore spaces. A critical parameter was the rigorous exclusion of water and molecular oxygen from the reaction medium. Without proper solvent treatment, undesired CuO_x species formed during exfoliation. However, under anhydrous conditions, the exfoliation process yields well-defined, Cu-containing, PTI nanosheets that maintain their metal−ligand network structure and dramatically increase the available surface area of the crystalline carbon nitride material. Thus, these results establish a viable synthetic route for producing two-dimensional carbon nitride materials with integrated catalytic sites, offering potential applications in heterogeneous catalysis and photocatalysis

■ ASSOCIATED CONTENT

Supporting Information

The Supporting Information is available free of charge at https://pubs.acs.org/doi/10.1021/acs.langmuir.5c05167.

Additional information and data regarding materials, methods, and analytical measurements concerning crystalline carbon nitride synthesis, exfoliation, and analysis (PDF)

■ AUTHOR INFORMATION

Corresponding Author

Paul A. Maggard − *Department of Chemistry and Biochemistry, Baylor University, Waco, Texas 76798, United States;* orcid.org/0000-0002-3909-1590; Email: Paul_Maggard@baylor.edu

Authors

Scott McGuigan − *Department of Chemistry and Biochemistry, Baylor University, Waco, Texas 76798, United States;* orcid.org/0000-0002-9554-0151

Erika Ortega Ortiz − *Department of Materials Science and Engineering, University of Pennsylvania, Philadelphia, Pennsylvania 19104, United States*

Sungho Jeon − *Department of Materials Science and Engineering, University of Pennsylvania, Philadelphia, Pennsylvania 19104, United States*

Carrie L. Donley − *Department of Chemistry, University of Chapel Hill, Chapel Hill, North Carolina 27599, United States;* orcid.org/0000-0003-0906-306X

Eric A. Stach − *Department of Materials Science and Engineering, University of Pennsylvania, Philadelphia, Pennsylvania 19104, United States;* orcid.org/0000-0002-3366-2153

Complete contact information is available at: https://pubs.acs.org/10.1021/acs.langmuir.5c05167

Author Contributions

#Scott McGuigan and Erika Ortega Ortiz are co-first authors.

Notes

The authors declare no competing financial interest.

■ ACKNOWLEDGMENTS

This material is based upon work solely supported as part of the Center for Hybrid Approaches in Solar Energy to Liquid Fuels (CHASE), an energy innovation hub funded by the U.S. Department of Energy, Office of Science, Office of Basic Energy Sciences under award number DE-SC0021173. STEM analysis was carried out at the Singh Center for Nanotechnology, which is supported by the NSF National Nanotechnology Coordinated Infrastructure Program under grant NNCI-2025608 and the Laboratory for Research on the Structure of Matter (MRSEC) supported by the National Science Foundation (DMR-2309043). XPS analysis was performed at the Chapel Hill Analytical and Nanofabrication Laboratory, CHANL, a member of the North Carolina Research Triangle Nanotechnology Network, RTNN, which is supported by the National Science Foundation, grant ECCS-2025064, as part of the National Nanotechnology Coordinated Infrastructure, NNCI.

■ REFERENCES

(1) Mazzanti, S.; Savateev, A. Emerging Concepts in Carbon Nitride Organic Photocatalysis. *ChemPlusChem.* **2020**, *85*, 2499−2517.

(2) Ding, Z.; Chen, X.; Antonietti, M.; Wang, X. Synthesis of Transition Metal-Modified Carbon Nitride Polymers for Selective Hydrocarbon Oxidation. *ChemSusChem* **2011**, *4*, 274−281.

(3) Colombari, F. M.; da Silva, M. A. R.; Homsi, M. S.; de Souza, B. R. L.; Araujo, M.; Francisco, J. L.; da Silva, G. T. S. T.; Silva, I. F.; de Moura, A. F.; Teixeira, I. F. Graphitic Carbon Nitrides as Platforms for Single-Atom Photocatalysis. *Faraday Discuss.* **2021**, *227*, 306−320.

(4) Li, Y.; Li, B.; Zhang, D.; Cheng, L.; Xiang, Q. Crystalline Carbon Nitride Supported Copper Single Atoms for Photocatalytic CO_2 Reduction with Nearly 100% CO Selectivity. *ACS Nano* **2020**, *14*, 10552−10561.

(5) Fu, J.; Zhu, L.; Jiang, K.; Liu, K.; Wang, Z.; Qiu, X.; Li, H.; Hu, J.; Pan, H.; Lu, Y.-R.; Chan, T.-S.; Liu, M. Activation of CO_2 on Graphitic Carbon Nitride Supported Single-Atom Cobalt Sites. *Chem. Eng. J.* **2021**, *415*, No. 128982.

(6) Genoux, A.; Pauly, M.; Rooney, C. L.; Choi, C.; Shang, B.; McGuigan, S.; Fataftah, M. S.; Kayser, Y.; Suhr, S. C. B.; DeBeer, S.; Wang, H.; Maggard, P. A.; Holland, P. L. Well-Defined Iron Sites in Crystalline Carbon Nitride. *J. Am. Chem. Soc.* **2023**, *145*, 20739−20744.

(7) Pauly, M.; White, E.; Deegbey, M.; Fosu, E. A.; Keller, L.; McGuigan, S.; Dianat, G.; Gabilondo, E.; Wong, J. C.; Murphey, C. G. E.; Shang, B.; Wang, H.; Cahoon, J. F.; Sampaio, R.; Kanai, Y.; Parsons, G.; Jakubikova, E.; Maggard, P. A. Coordination of Copper within a Crystalline Carbon Nitride and Its Catalytic Reduction of CO_2. *Dalt. Trans.* **2024**, *53*, 6779−6790.

(8) Huang, P.; Huang, J.; Pantovich, S. A.; Carl, A. D.; Fenton, T. G.; Caputo, C. A.; Grimm, R. L.; Frenkel, A. I.; Li, G. Selective CO_2 Reduction Catalyzed by Single Cobalt Sites on Carbon Nitride under Visible-Light Irradiation. *J. Am. Chem. Soc.* **2018**, *140*, 16042−16047.

(9) Zhang, G.; Huang, C.; Wang, X. Dispersing Molecular Cobalt in Graphitic Carbon Nitride Frameworks for Photocatalytic Water Oxidation. *Small* **2015**, *11*, 1215−1221.

(10) Kessler, F. K.; Schnick, W. From Heptazines to Triazines − On the Formation of Poly(Triazine Imide). *Z. Anorg. Allg. Chem.* **2019**, *645*, 857−862.
(11) Chong, S. Y.; Jones, J. T. A.; Khimyak, Y. Z.; Cooper, A. I.; Thomas, A.; Antonietti, M.; Bojdys, M. J. Tuning of Gallery Heights in a Crystalline 2D Carbon Nitride Network. *J. Mater. Chem. A: Mater.* **2013**, *1*, 1102−1107.
(12) Cypher, S. M.; Pauly, M.; Castro, L. G.; Donley, C. L.; Maggard, P. A.; Goldberg, K. I. Ethanol Upgrading to N-Butanol Using Transition-Metal-Incorporated Poly(Triazine)Imide Frameworks. *ACS Appl. Mater. Interfaces* **2023**, *15*, 36384−36393.
(13) Xu, J.; Zhang, L.; Shi, R.; Zhu, Y. Chemical Exfoliation of Graphitic Carbon Nitride for Efficient Heterogeneous Photocatalysis. *J. Mater. Chem. A: Mater.* **2013**, *1*, 14766−14772.
(14) Li, Y.; Wang, M.-Q.; Bao, S.-J.; Lu, S.; Xu, M.; Long, D.; Pu, S. Tuning and Thermal Exfoliation Graphene-like Carbon Nitride Nanosheets for Superior Photocatalytic Activity. *Ceram. Int.* **2016**, *42*, 18521−18528.
(15) Jia, J.; White, E. R.; Clancy, A. J.; Rubio, N.; Suter, T.; Miller, T. S.; McColl, K.; McMillan, P. F.; Brázdová, V.; Corà, F.; Howard, C. A.; Law, R. V.; Mattevi, C.; Shaffer, M. S. P. Fast Exfoliation and Functionalization of Two-Dimensional Crystalline Carbon Nitride by Framework Charging. *Angew. Chem. Int. Ed.* **2018**, *57*, 12656−12660.
(16) Burmeister, D.; Müller, J.; Plaickner, J.; Kochovski, Z.; List-Kratochvil, E. J. W.; Bojdys, M. J. Size Effects of the Anions in the Ionothermal Synthesis of Carbon Nitride Materials. *Chem.—Eur. J.* **2022**, *28*, No. e202200705.
(17) Burmeister, D.; Eljarrat, A.; Guerrini, M.; Röck, E.; Plaickner, J.; Koch, C. T.; Banerji, N.; Cocchi, C.; List-Kratochvil, E. J. W.; Bojdys, M. J. On the Non-Bonding Valence Band and the Electronic Properties of Poly (Triazine Imide), a Graphitic Carbon Nitride. *Chem. Sci.* **2023**, *14*, 6269−6277.
(18) Villalobos, L. F.; Vahdat, M. T.; Dakhchoune, M.; Nadizadeh, Z.; Mensi, M.; Oveisi, E.; Campi, D.; Marzari, N.; Agrawal, K. V. Large-Scale Synthesis of Crystalline g-C_3N_4 Nanosheets and High-Temperature H_2 Sieving from Assembled Films. *Sci. Adv.* **2023**, *6*, No. eaay9851.
(19) Momma, K.; Izumi, F. VESTA3 for Three-Dimensional Visualization of Crystal, Volumetric and Morphology Data. *J. Appl. Crystallogr.* **2011**, *44*, 1272−1276.
(20) Pauly, M.; Kröger, J.; Duppel, V.; Murphey, C.; Cahoon, J.; Lotsch, B. V.; Maggard, P. A. Unveiling the Complex Configurational Landscape of the Intralayer Cavities in a Crystalline Carbon Nitride. *Chem. Sci.* **2022**, *13*, 3187−3193.
(21) Mallik, M.; Monia, S.; Gupta, M.; Ghosh, A.; Toppo, M. P.; Roy, H. Synthesis and Characterization of Cu_2O Nanoparticles. *J. Alloys Compd.* **2020**, *829*, No. 154623.
(22) Sahooli, M.; Sabbaghi, S.; Saboori, R. Synthesis and Characterization of Mono Sized CuO Nanoparticles. *Mater. Lett.* **2012**, *81*, 169−172.
(23) Singh, D. P.; Ojha, A. K.; Srivastava, O. N. Synthesis of Different $Cu(OH)_2$ and CuO (Nanowires, Rectangles, Seed-, Belt-, and Sheetlike) Nanostructures by Simple Wet Chemical Route. *J. Phys. Chem. C* **2009**, *113*, 3409−3418.
(24) Fornaro, T.; Burini, D.; Biczysko, M.; Barone, V. Hydrogen-Bonding Effects on Infrared Spectra from Anharmonic Computations: Uracil−Water Complexes and Uracil Dimers. *J. Phys. Chem. A* **2015**, *119*, 4224−4236.
(25) Suter, T. M.; Miller, T. S.; Cockcroft, J. K.; Aliev, A. E.; Wilding, M. C.; Sella, A.; Corà, F.; Howard, C. A.; McMillan, P. F. Formation of an Ion-Free Crystalline Carbon Nitride and Its Reversible Intercalation with Ionic Species and Molecular Water. *Chem. Sci.* **2019**, *10*, 2519−2528.
(26) Liu, M.; Wei, C.; Zhuzhang, H.; Zhou, J.; Pan, Z.; Lin, W.; Yu, Z.; Zhang, G.; Wang, X. Fully Condensed Poly (Triazine Imide) Crystals: Extended π-Conjugation and Structural Defects for Overall Water Splitting. *Angew. Chem., Int. Ed.* **2022**, *61*, No. e202113389.
(27) Liang, X.; Xue, S.; Yang, C.; Ye, X.; Wang, Y.; Chen, Q.; Lin, W.; Hou, Y.; Zhang, G.; Shalom, M.; Yu, Z.; Wang, X. The Directional Crystallization Process of Poly (Triazine Imide) Single Crystals in Molten Salts. *Angew. Chem., Int. Ed.* **2023**, *62*, No. e202216434.
(28) McGuigan, S.; Tereniak, S. J.; Donley, C. L.; Smith, A.; Jeon, S.; Zhao, F.; Sampaio, R. N.; Pauly, M.; Keller, L.; Collins, L.; Parsons, G. N.; Lian, T.; Stach, E. A.; Maggard, P. A. Discovery of a Hybrid System for Photocatalytic CO_2 Reduction via Attachment of a Molecular Cobalt-Quaterpyridine Complex to a Crystalline Carbon Nitride. *ACS Appl. Energy Mater.* **2023**, *6*, 10542−10553.
(29) McGuigan, S.; Tereniak, S. J.; Smith, A.; Jana, S.; Donley, C. L.; Collins, L.; Ghorai, N.; Xu, Y.; Fosu, E. A.; Suhr, S.; Margavio, H. R. M.; Yang, H.; Parsons, G. N.; Holland, P. L.; Jakubikova, E.; Lian, T.; Maggard, P. A. Illuminating the Mechanistic Impacts of an Fe-Quaterpyridine Functionalized Crystalline Poly (Triazine Imide) Semiconductor for Photocatalytic CO_2 Reduction. *Inorg. Chem. Front.* **2025**, *12*, 6640−6654.
(30) Gurevich, A. B.; Bent, B. E.; Teplyakov, A. V.; Chen, J. G. A NEXAFS Investigation of the Formation and Decomposition of CuO and Cu_2O Thin Films on Cu(100). *Surf. Sci.* **1999**, *442*, L971−L976.
(31) Gleason, S. P.; Lu, D.; Ciston, J. Prediction of the Cu Oxidation State from EELS and XAS Spectra Using Supervised Machine Learning. *NPJ. Comput. Mater.* **2024**, *10*, 221.

https://doi.org/10.1021/acs.langmuir.5c05167
Langmuir 2026, 42, 4489−4496